Interferometer Design and Application: Measuring Helium-Neon Laser Wavelength and Index of Refraction of Air and Glass with Michelson and Fabry-Perot Interferometers with an Additional Investigation and Review of Twyman-Green Interferometer Design

Milo Brown
Department of Physics, University of California, Santa Barbara, CA 93106
(Dated: February 1, 2024)

Interferometers use phase-shift interference to measure small changes in distance and changes in medium with high precision. We used Michelson and Fabry-Perot interferometers to measure the wavelength of a Helium-Neon laser and the indices of refraction of air and glass. We found the wavelength of the Helium-Neon laser to be 643±1004 nanometers using the Michelson interferometer and 649±1003 nanometers using the Fabry-Perot interferometer. These values are consistent with the theoretical wavelength, with a low statistical uncertainty and high equipment uncertainty due to the measurement accuracy of the displacement of the movable mirror. Using a Michelson interferometer, we found the index of refraction of air to be 1.000206 ± 0.000044. This is within 0.0064% of the expected value; however, it is not consistent with the expected value due to the low uncertainty. We found the refractive index of glass at 1.15 ± 0.08. This is inconsistent with our expected value of 1.5 due to an error in our counting method.

I. INTRODUCTION

From gravitational waves [1] to quantum information, interferometry pioneers the forefront of experimental physics. Therefore, an undergraduate introduction to interferometry configuration and experimental design allows young physicists to develop essential and adaptable skills in optics and related fields. Composed of three undergraduates, our experimental group investigated the properties of several interferometer designs–Michelson, Fabry-Perot, and Twyman-Green–and used each interferometer in several experiments, such as measuring the effects of changing path length and refractive materials on the interference pattern characteristic of these interferometer designs.

In its most basic conception, an interferometer is a device that uses the interference between two or more waves (note that we refer to the classical interpretation of light because our Helium Neon laser provided a coherent stream of photons rather than a quantum single-photon scenario) to detect changes in parameters with relatively high precision. For example, we can detect changes in the length of an arm of a Michelson interferometer by observing the transitions in the interference fringe pattern; this pattern is demonstrated both theoretically and experimentally in Figure 1. The interference fringe pattern appears when the light (which has wavelike properties and can be considered a wave for our purposes) interferes with light of a different phase. As a reminder, when two waves interfere, they can interfere constructively or destructively, creating areas in the resulting wave pattern where there is a higher amplitude and areas where the amplitude of the light is diminished or suppressed.

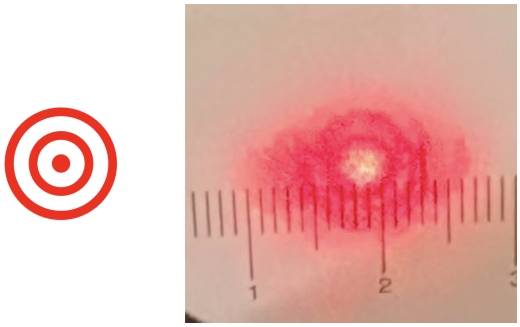

FIG. 1: The figure above shows a theoretical depiction of interference fringes on the left and our experimental fringes found using a Michelson interferometer on the right. The fidelity of the camera introduces a level of visual error to the picture on the right that was not present in the original experiment.

A. Theory and Background of Experimental Methods

Although each interferometer design shares certain qualities, such as the interference pattern (which changes with the relative phase of the light sources) the Michelson, Fabry-Perot, and Twyman-Green interferometer configurations are arranged in different ways and are optimal in different applications. The following sections will introduce each interferometer design and discuss some of their relative strengths.

1. Michelson Interferometer

Since its conception and immediate failure to detect a medium through which light must travel (i.e., the "luminous aether"), the Michelson interferometer has proved experimentally useful and has inspired design variations with specific applications (such as the Twyman-Green interferometer). For example, the laser interferometer gravitational wave observatory (LIGO) uses a large Michelson interferometer to detect the distortion of spacetime after two massive stellar objects collide [1].

In a Michelson interferometer, light travels to a 50/50 beam splitter, where half the light is reflected and half is transmitted. Whether the light reflects or transmits, the light travels from the beam splitter to a mirror, reflecting the light back to the beam splitter, which combines the light from both paths. The resulting interference pattern allows experimentalists to measure small changes in distance or the effective speed of light through a medium. This interferometer design is shown in Figure 2.

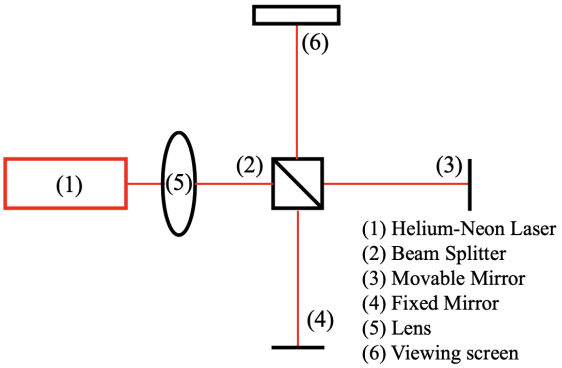

FIG. 2: This labeled diagram and experimental setup of a Michelson interferometer demonstrates how coherent laser light will reflect and transmit through a beam splitter and travel along each arm of the interferometer before recombining at the viewing screen.

Notice that the movable mirror can move towards and away from the beam splitter, adjusting the path length of the light and shifting the phase, thereby initiating a fringe transition. In our experiment, we observed the fringe transitions as we decreased the distance between the movable mirror and the beam splitter to find the wavelength of the light, which is governed by Equation 1, where λ represents the wavelength of the light, d_m represents the distance the mirror moved towards the beam splitter, and N represents the number of fringe transitions.

$$\lambda = 2d_m/N \tag{1}$$

Although the "luminous aether" does not exist, the Michelson interferometer can still be used to measure the effects of different mediums on the relative phase of light, allowing for accurate measurements of index of refraction for different mediums, including air. In our experiment, we used a vacuum cell to measure the changes in fringe transitions as the air drained from the cell. The slope of the refractive index versus pressure graph is governed by equation 2, where P_i and P_f are the initial and final pressures of the air, n_i and n_f are the refractive indices of the air at P_i and P_f, N is the number of fringe transitions counted as air leaves the cell, λ_0 is the wavelength of the light in a vacuum, and d is the length of the vacuum cell (3.0 cm).

$$\frac{n_i - n_f}{P_i - P_f} = \frac{N\lambda_0}{2d(P_i - P_f)} \tag{2}$$

Using this equation to find the slope of the index of refraction of air at different pressures and the fact that the refractive index of a vacuum is 1, we can create a linear relationship between the refractive index and the pressure and use this relationship to find the index of refraction of air at any pressure.

We can also use a Michelson interferometer to find the refractive index of glass. To calculate the refractive index of glass, we rotated a glass plate to different angles and measured the fringe transitions at each angular rotation. The index of refraction of glass is governed by Equation 3, where θ is the angle to which the glass is rotated and t is the thickness of the glass (3 mm).

$$n = \frac{(2t - N\lambda_0)(1 - \cos\theta)}{2t(1 - \cos\theta) - N\lambda_0} \tag{3}$$

2. Fabry-Perot Interferometer

Although LIGO's gravitational-wave-detecting Michelson interferometer has an arm length of 4 kilometers, Fabry-Perot cavities increase the effective arm length to 1200 kilometers. Fabry-Perot interferometers increase measurement accuracy by using multiple reflections of light between two mirrors to increase the effective path length of the light. Therefore, we expect results from Fabry-Perot interferometers to be more accurate than measurements from Michelson interferometers.

A Fabry-Perot interferometer consists of two parallel mirrors; the distance between these mirrors determines the resonance frequency of the cavity. When we change the distance between the parallel mirrors, we observe fringe transitions, which allow us to measure the wavelength of the source using Equation 1. Figure 3 shows a theoretical diagram of a Fabry-Perot interferometer.

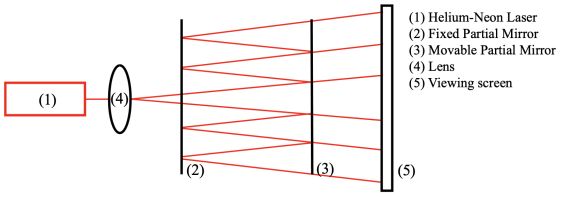

FIG. 3: The Fabry-Perot interferometer consists of a cavity between two parallel mirrors.

3. *Twyman-Green Interferometer*

A Twyman-Green interferometer is a variant of a Michelson interferometer that is largely used to test optical components [2]. We constructed a Twyman-Green interferometer in addition to the Michelson and Fabry-Perot interferometers required for our experimental measurements to investigate a tertiary interferometer design and expand our understanding of interferometry composure. Figure 4 shows our Twyman-Green setup, which includes an additional lens in front of the movable mirror. This additional lens allows us to investigate wavefront quality (and thereby surface shape of optical components) [3].

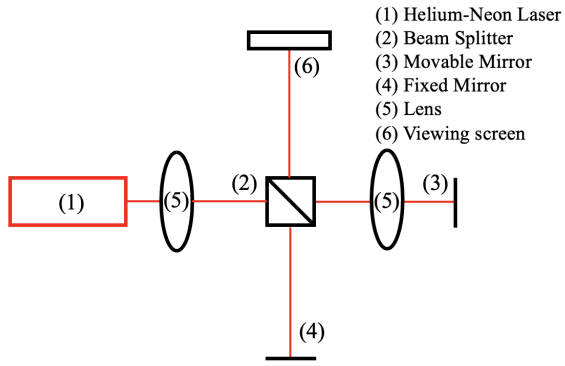

FIG. 4: The Twyman-Green interferometer is a variation of the Michelson interferometer with an additional lens in front of the movable mirror.

II. METHODS

A. Experimental Methods: Calibration

Although I explained how the measurements were taken and described our experimental apparatus in previous sections, it is necessary to briefly discuss the calibration of the laser before presenting our raw experimental data.

To align the laser, we adjusted the angle of the laser source to ensure the laser pointed directly at the source when reflected by a mirror that was perpendicular to the laser's path. With a correctly aligned laser, we found clear and distinct interference fringes.

B. Raw Data

Using the Michelson interferometer, we found the displacement values per 20 fringe transitions in Table I over 3 trials. The data from the third trial differs somewhat from the data from the first 2 trials, indicating a possible outlier.

TABLE I: Displacement (μm) over intervals of 20 Fringe Transitions Using a Michelson interferometer

Fringes	Displacement: Trial 1	Trial 2	Trial 3
20	6.5 ± 0.5	6.5 ± 0.5	8.2 ± 0.5
40	12.2 ± 0.5	12.7 ± 0.5	15.2 ± 0.5
60	18.2 ± 0.5	18.9 ± 0.5	21.9 ± 0.5
80	24.0 ± 0.5	25.2 ± 0.5	28.2 ± 0.5
100	30.1 ± 0.5	31.5 ± 0.5	34.7 ± 0.5
120	36.1 ± 0.5	37.8 ± 0.5	41.0 ± 0.5
140	42.7 ± 0.5	44.7 ± 0.5	47.4 ± 0.5
160	49.8 ± 0.5	51.0 ± 0.5	53.7 ± 0.5
180	55.6 ± 0.5	57.2 ± 0.5	60.6 ± 0.5
200	61.9 ± 0.5	63.6 ± 0.5	67.5 ± 0.5
220	68.4 ± 0.5	70.1 ± 0.5	74.2 ± 0.5
240	74.9 ± 0.5	76.5 ± 0.5	81.0 ± 0.5
260	81.2 ± 0.5	82.9 ± 0.5	88.0 ± 0.5
280	87.4 ± 0.5	88.9 ± 0.5	95.1 ± 0.5
300	93.5 ± 0.5	95.2 ± 0.5	102.0 ± 0.5

Table II shows the same data for the Fabry-Perot interferometer.

As we evacuated the vacuum chamber, we found the fringe transitions in Table III over 3 trials.

Table IV shows the number of fringe transitions at different angle changes of glass over 3 trials per each angle.

III. RESULTS

We used the slope of number of fringe transitions compared to the change in distance doubled (e.g., $\frac{2\Delta d_m}{N}$) to calculate the wavelength of the Helium-Neon laser in Figure 5.

The statistical error for the linear regression is 0.004 micrometers. The expected error for the equipment is 0.5 micrometers for a small change in distance; since our result relies on twice that distance, the uncertainty is doubled as well. Therefore

TABLE II: Displacement (μm) over intervals of 20 Fringe Transitions Using a Fabry-Perot interferometer

Fringes	Displacement: Trial 1	Trial 2	Trial 3
20	8.4 ± 0.5	9.1 ± 0.5	7.0 ± 0.5
40	14.8 ± 0.5	15.1 ± 0.5	13.6 ± 0.5
60	22.7 ± 0.5	22.0 ± 0.5	19.9 ± 0.5
80	29.5 ± 0.5	28.7 ± 0.5	25.8 ± 0.5
100	36.1 ± 0.5	35.6 ± 0.5	32.3 ± 0.5
120	42.6 ± 0.5	41.9 ± 0.5	39.0 ± 0.5
140	48.5 ± 0.5	47.9 ± 0.5	45.1 ± 0.5
160	55.7 ± 0.5	54.2 ± 0.5	51.5 ± 0.5
180	62.0 ± 0.5	60.8 ± 0.5	58.1 ± 0.5
200	68.8 ± 0.5	67.2 ± 0.5	64.2 ± 0.5
220	74.5 ± 0.5	73.7 ± 0.5	72.5 ± 0.5
240	81.1 ± 0.5	80.0 ± 0.5	79.0 ± 0.5
260	87.2 ± 0.5	86.4 ± 0.5	85.5 ± 0.5
280	93.6 ± 0.5	92.5 ± 0.5	91.8 ± 0.5
300	99.6 ± 0.5	99.1 ± 0.5	98.1 ± 0.5

TABLE III: Number of Fringe Transitions as Pressure (inHg) Decreases Over 3 Trials

Pressure	Fringe Transitions: Trial 1	Trial 2	Trial 3
5.00 ± 0.25	3	3	4
10.00 ± 0.25	7	7	6
15.00 ± 0.25	10	10	9
20.00 ± 0.25	13	14	12
25.00 ± 0.25	16	17	15

TABLE IV: Number of Fringe Transitions as Angle (degrees) Increases from 0 to a Range of Angles Over 3 Trials

Angle	Fringe Transitions: Trial 1	Trial 2	Trial 3
10.0 ± 0.3	89	95	114
11.0 ± 0.3	92	91	92
12.0 ± 0.3	95	102	103
13.0 ± 0.3	124	122	130

the measured wavelength is 643±1004 nanometers. The expected wavelength of a Helium-Neon laser is 632.8 nanometers. Although this is well within the expected uncertainty range, it must be acknowledged that the uncertainty range is rather large.

We can use the same analysis technique to find the wavelength using the Fabry-Perot interferometer in Figure 6.

The statistical error for the linear regression is 0.003 micrometers. The equipment error introduced by the movement of the movable mirror is the same as the Michelson interferometer. Therefore the measured wavelength is 649±1003 nanometers. This is further from the expected theoretical value than the Michelson, but the theoretical value is still well within the uncertainty.

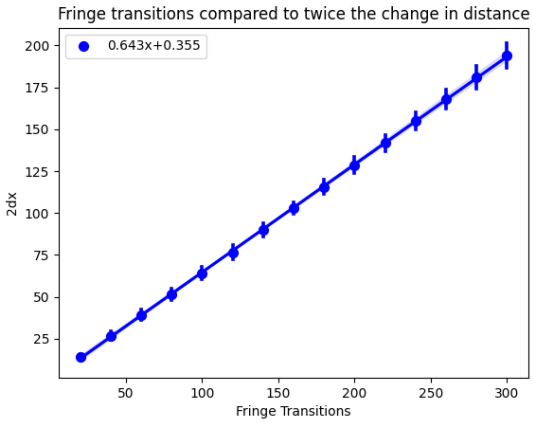

FIG. 5: The graph shows the calculation for the wavelength of the Helium-Neon laser using a Michelson interferometer using the slope of a linear regression fit. I used a linear regression model on the average of all three trials. The error introduced by taking the average increases as the fringe transitions increase because each possible lapse in precision from each fringe transition element increases the total lack of precision in later measurements. The error bars reflect this, and the confidence interval spreads near the higher fringe transition measurements.

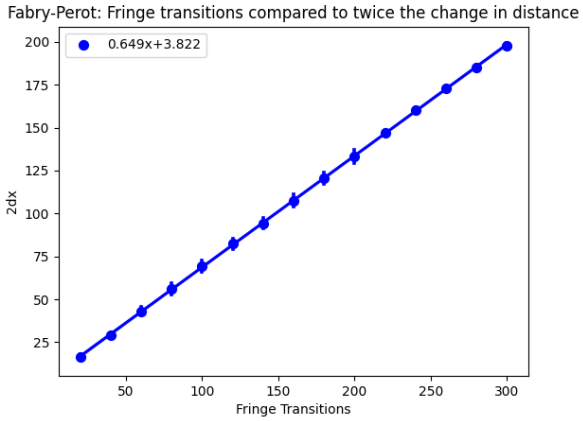

FIG. 6: The graph shows the calculation for the wavelength of the Helium-Neon laser using a Fabry-Perot interferometer. The confidence interval is narrow throughout the graph, and the statistical uncertainty maximizes near the middle of the graph rather than the end. The lower statistical uncertainty might be explained by the longer path length of the light in a Fabry-Perot interferometer.

Using our raw data, we can average the slope of the refractive index of air at different pressures to graph the change of refractive index at different air pressures and measure the refractive index of air at atmospheric pressure. Since the uncertainty of each measurement is 0.25 inches Hg, the uncertainty of our slope is determined by scaling the uncertainty using the constants from our function and then finding the mean uncertainty $\frac{\Delta}{\sqrt{n}}$. We find the refractive index of air at atmospheric pressure to be 1.000206 $\pm$ 0.000044.

The most accurate measurement of the index of refraction of glass should be calculated from the largest change of angle. We find the average of the calculated refractive indices at 13.0 $\pm$ 0.3 to be 1.15 $\pm$ 0.08. We first find the mean equipment uncertainty $\frac{\Delta}{\sqrt{n}} = 0.1$ of the angle and the mean statistical uncertainty of the fringe transitions $\frac{\sqrt{\frac{1}{n-1}\sum(x_i-\bar{x})^2}}{\sqrt{n}} \approx 2.4037$. Then, using error propagation, we find the uncertainty of the refractive index to be 0.08.

IV. DISCUSSION

The measurement of the wavelength from the Fabry-Perot interferometer has a lower uncertainty than the Michelson interferometer, but is farther from the expected value. Some discrepancies between the experimental and expected wavelengths may be introduced by thermal instability and differences between the ideal and experimental laser. There may also be more opportunities for human error when counting the fringes of the Fabry-Perot because the intensity of the Fabry-Perot fringes are lower and the interference fringes are smaller and less dramatic.

Our measured index of refraction of air at atmospheric pressure differs from the expected value by 0.0064%. However, the uncertainty does not appear to account for this small difference. This may be due to the fluctuations in the relative angle of the vacuum cell with respect to the path of the light, which may have introduced some aberration due to the refractive index of glass.

Our measured refractive index of glass, 1.15 $\pm$ 0.08, was significantly far from the expected value of 1.5. This is likely due to an error in our counting method. Since we found counting a large number of fringe transitions difficult due to eye strain, we decided to record the fringe transitions and count them using a slow motion camera. However, a significant number of fringe transitions may have been lost or left uncounted due to the unreliability of this methodology.

ACKNOWLEDGMENTS

I would like to thank my lab partners, Ananda Guha and Kenny Zhou, for collaborating to thoroughly investigate properties of interferometers. I would also like to thank our teaching assistant, Zihang Wang, for helping us collaborate as a cohesive group and providing guidance when necessary.

[1] "LIGO's Interferometer," (n.d.).
[2] D. Malacara, en"Twyman–Green Interferometer," in en*Optical Shop Testing* (John Wiley & Sons, Ltd, 2007) pp. 46–96, section: 2 _eprint: https://onlinelibrary.wiley.com/doi/pdf/10.1002/9780470135976.ch2.
[3] Dr Rüdiger Paschotta, en"Twyman–Green interferometers,".